Towards Thermal Flowsensing With pL/s Resolution

N.R.Tas, T.S.J. Lammerink, P.J. Leussink, J.W. Berenschot, H-E. de Bree, M. Elwenspoek
MESA+ Research Institute, Department of Electrical Engineering, University of Twente, P.O. Box 217, 7500 AE Enschede, The Netherlands. E-mail: n.r.tas@el.utwente.nl.

Abstract: This paper focuses on the development of highly sensitive calorimetric flow sensors. Both the hydrodynamics of the flow channel, as well as the heat transfer are analyzed in detail. With the expressions for the hydraulic resistance of the flow channel and the hydraulic system requirements for the flow sensor, it is possible to optimize the design of the flow channel. It is theoretically shown why for small v the calorimetric flow sensor output is linear in v. Also it follows from theory that for a symmetrical configuration, in this linear regime the heater temperature is independent of v for constant heating power. This suggests that for low Reynolds Number, King's Law has to be modified. Different configurations and methods are analyzed: absolute, differential, two beam, three beam, CPA, CTA and TBA. The latter is a real thermal balance measurement and allows the use of non-linear sensing elements. From our experience with acoustical measurements it is possible to estimate practical attainable sensitivity. In combination with proper flow channel design, and a fabrication technology for narrow channels, it is shown that pL/s sensitivity is in reach.

Keywords: Thermal flow sensors, anemometry, calorimetric flow sensors.

1. Introduction

This papers investigates the modeling, design and performance of silicon micromachined thermal flow sensors, with a focus on high sensitivity. Our motivation for the development of highly sensitive flow sensors, with a resolution down to pL/s, is the application in micro-chemical systems (MICS), where accurate dosing of chemicals is desired. In section 6 flow sensor design for this application will be addressed briefly. The measurement of flow using thermal principles has been widely used throughout the whole 20th century. The convective cooling of an electrically heated wire was already described extensively by King [1] in 1914. The first sensors were of the hot wire anemometer type. This principle is based on measurement of the amount of heat injected from a heated object into the flowing medium. In the early seventies for the first thermal flow sensors were made by silicon micromachining [2]. A big improvement in sensor sensitivity and power efficiency could be obtained by fabrication of (poly-)silicon or silicon nitride micro-bridges, for well-isolated suspension of the temperature sensing elements as well as heaters [3,4,5]. According to Bradshaw [6] in his review of thermal flow sensors, the first *calorimeter flow sensors* were realized in the 1950's. The basic operation principle for the static thermal driving mode, is the convective disturbance of the zero flow temperature distribution around a heater which is maintained by heat conduction to the heat sinks. The disturbance is measured by one or two temperature sensors at some distance of the heater. Characteristic for this type of flow sensor is a differential sensitivity larger than zero around $v = 0$. We will analyze the heat transfer in this type of sensor, to show that for small v the sensor output is proportional to v. Fabricated using silicon micromachining the calorimetric flow sensors can be made extremely sensitive [7,8,9]. Therefore the focus of this paper will be on this principle. Calorimetric flow sensors can also be operated in a dynamic thermal mode, the *time of flight flow sensors*: heat pulses generated at the heater are transported with the moving fluid. During the transport to a temperature sensor at distance l down-stream from the heater, the pulse will broaden. Roughly, for flow velocities smaller than $v_c = D_T / l$ the signal tends to be too broad to be useful [10], where D_T is the thermal diffusion coefficient [m^2/s].
Besides heat transfer, significant attention is paid to the design of the flow channel of the sensor (section 2). With a optimization of this channel, within the boundary conditions given by the fluidic system design, the sensor sensitivity can be largely increased. The example given in section 6 illustrates this.

2. Hydrodynamic and Thermal Modeling

In this section hydrodynamics and heat transfer in basic configurations are analyzed. For the sake of simplicity all analyses are done under the assumption of Newtonian fluids with constant density and constant viscosity.

Laminar Flow Velocity Distribution, fully developed flow

For a stationary, fully developed laminar flow in a tube of constant cross section, under the conditions of a Newtonian fluid with constant density and viscosity, the momentum balance (Navier-Stokes equations) reduces to [11]:

$$\mu \nabla^2 v = \nabla p \qquad (1)$$

Where μ is the fluid viscosity [Nsm^{-2}], p is the pressure and v is the flow velocity. In general the differential equation is solved under the boundary conditions $v = 0$ at the wall, and shear stress $\tau = 0$ at the center line of the tube. For a circular tube the well known parabolic flow profile results [12]:

$$u(r) = \frac{r_0^2}{4\mu} \cdot (-\frac{\mathrm{d}p}{\mathrm{d}x})(1 - \frac{r^2}{r_0^2}) \qquad (2)$$

With r and r_0 the radial distance from the center line of the tube, and the inner-radius of the tube respectively, and $\mathrm{d}p / \mathrm{d}x$ the longitudinal pressure gradient. The condition for laminar flow can be given in a value of the dimensionless Reynolds number, which is defined as the ratio of the inertia and the viscous forces working on the fluid in a channel with diameter D:

$$Re_{\mathrm{D}} = \frac{\rho \cdot v_m \cdot D}{\mu} \qquad (3)$$

Where v_{m} is the mean fluid velocity, and ρ is the density of the fluid. The condition for the flow in a circular channel to be laminar is that Re_{D} is smaller than roughly 2000 [11].

Hydraulic resistance

Knowing the velocity distribution, the pressure drop across the tube can be calculated from a force balance: The shear stress at the tube wall times the contact area of the fluid plug with the wall is balanced by the pressure difference acting on the front and end surface of the fluid plug. This has been analyzed for different tube cross section, resulting in a general expression for the hydraulic resistance R (= pressure drop Δp divided by volume flow φ) [13]:

$$R = \frac{2k_{\mathrm{shape}} L}{D_{\mathrm{h}}^2 \cdot A} \cdot \mu \qquad [\mathrm{Nsm}^{-5}] \qquad (4)$$

Where $k_{\mathrm{shape}} = f \cdot Re$ a dimensionless constant depending on the cross sectional shape of the channel only [14, 15], D_{h} is the hydrodynamic diameter, L is the length, and A is the area of the cross section of the tube. The hydrodynamic diameter is defined by $D_{\mathrm{h}} = 4A / P$ with P the perimeter of the cross section. The product $k_{\mathrm{shape}} = f \cdot Re$ of the Fanning friction factor f and Reynolds number Re has been tabulated for different cross sections [14], table 1.

Using eq. (3) Reynolds number can be expressed as a function of Δp and φ [m^3 /s]:

$$Re_{\mathrm{D}}(\varphi) = \frac{4 \cdot \rho \cdot \varphi}{\pi \cdot \mu \cdot D} \qquad (5a)$$

$$Re_{\mathrm{D}}(\Delta p) = \frac{\rho \cdot D^3 \cdot \Delta p}{32 \cdot \mu^2 \cdot l} \qquad (5b)$$

The resistance has been derived for fully developed laminar flow. It is only valid if the entrance length (the length along which the flow velocity distribution establishes) is small compared to the length of the tube. For a circular tube the entrance length is given by the following expression [14]:

$$\frac{L_{hy}}{D} = 0.59 + 0.056 \cdot Re_{\mathrm{D}} \qquad (6)$$

With $D = 2 \cdot r_0$ the diameter of the circular channel. The non-linearity stems from kinetic pressure losses, which are proportional to φ^2. As an example, we show measured pressure vs. flow characteristics of triangular microchannels (fig. 1) [13, 16]. For two channels with identical cross section and a length of 0.8 ± 0.1 and 2.8 ± 0.1 mm respectively, and a top

width $2a = 170 \pm 2$ µm, the curves are given in fig. 2. For the same pressure applied, the shorter channel shows more non-linearity. This can be explained by looking at the ratio L / L_{hy}. For the short channel $L / L_{hy} = 1.1$ and for the long channel $L / L_{hy} = 0.1$, both calculated for 8 kPa applied pressure. These entrance lengthes have been estimated using eq. (6), which is the expression for a circular tube. To use it for other cross sections, the diameter of the circular tube is replaced by the hydrodynamic diameter for the particular cross sections.

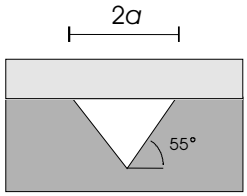

Figure 1: Cross section of the triangular microchannels used for the resistance measurement. The channel has been created by KOH etching of a <100> silicon wafer, and has been closed by anodic bonding of a glass wafer.

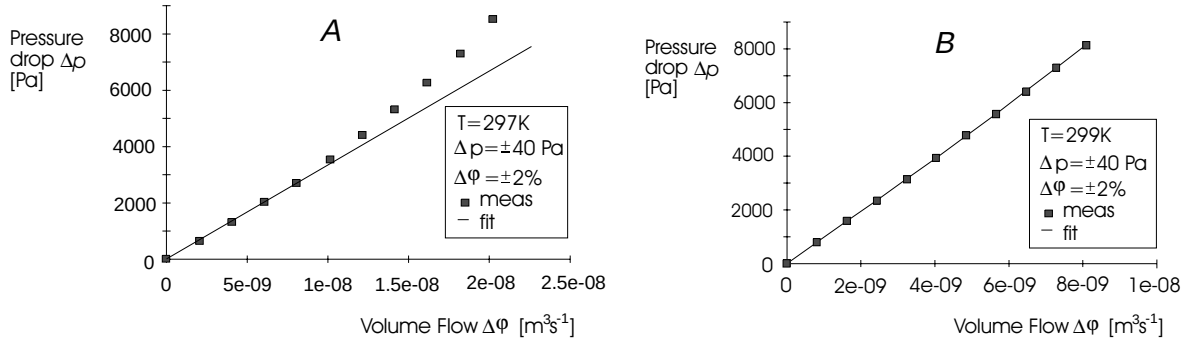

Figure 2: Measured pressure vs. flow characteristic of two channels with identical cross section, a length of 0.8 ± 0.1 mm (*A*) and 2.8 ± 0.1 mm (*B*) respectively, and a top width $2a = 170 \pm 2$ µm. Measurements have been done with ethanol (liquid).

Shape	**Shape const.** k_{shape}	**Hydrodynamic Diameter** D_h **[m]**	**Area** A **[m²]**	**Resistance** R **[Nsm⁻⁵]**
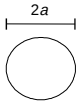	16	$2a$	πa^2	$\frac{8L}{\pi a^4}\mu$
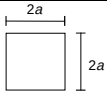	14.2	$2a$	$4a^2$	$\frac{1.78L}{a^4}\mu$
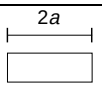	24	$4b$	$4ab$	$\frac{3L}{4ab^3}\mu$
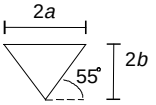	13.3	$1.04a$	$1.41a^2$	$\frac{17.4L}{a^4}\mu$

Table 1: Shape constant, the hydrodynamic diameter, the area of the cross section and the resistance for a length L [m] and a liquid viscosity µ [Nsm^{-2}].

To give a feeling for the dimensions, for a circular tube with an inner diameter of 0.1 mm and a length of 2 mm, the linear friction regime is roughly for Re < 300. This is within the laminar flow regime. The maximum allowed pressure and flow for Re < 300 follow from eq. (5a,b): For air (T = 293 K) $\Delta p_{max,\,air}$ = 0.05 Bar and $\varphi_{max,\,air}$ = 0.4 mL/s, and for water (T = 293 K) $\Delta p_{max,water}$ = 0.2 Bar and $\varphi_{max,water}$ = 0.02 mL/s.

Boundary layer theory

The flow boundary layer is the layer across which momentum is transferred. For a flat plate and a flow parallel to the plate, the boundary layer thickness $\delta(x)$ at a distance x from the leading edge of the plate is given by [11]:

$$\delta(x) = 4.64 \cdot \sqrt{\frac{\mu \cdot x}{\rho \cdot v_\infty}} \qquad (7)$$

Where v_∞ is the uniform flow velocity of the fluid far away from the plate. Similar, the thermal boundary layer is the layer across which the heat exchange with the fluid occurs. It can be seen as the penetration depth of the heat into the streaming fluid. For a fluid flowing parallel to a flat plate at uniform temperature elevation with respect to the incoming fluid, an expression similar to eq. (7) results for the thermal boundary layer thickness $\delta_T(x)$. Usually it is therefore given relative to the thickness of the flow boundary layer, according to:

$$\delta_T = \Delta \cdot \delta \qquad (8)$$

The ratio Δ is determined by the ratio of the thermal and the momentum diffusivity of the fluid, which is expressed by the dimensionless Prandl number: $Pr = c_p \cdot \mu / k$, with c_p the heat capacity of the fluid [J kg^{-1}K^{-1}]and k the heat conductivity [WK^{-1}m^{-1}]. For $Pr > 1$ the thickness ratio is given by [11]:

$$\Delta = Pr^{-1/3} \qquad (9)$$

Often for gases $Pr \approx 1$ and commonly $\delta_T = \delta$ is taken. For most liquids $Pr > 1$ and $\Delta < 1$ (the thermal boundary layer is thinner than the flow boundary layer). Figure 3 illustrates the shape of the boundary layers.

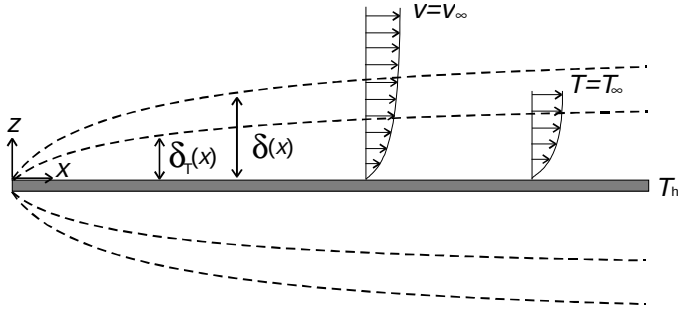

Figure 3: Flow δ, and thermal boundary layer thickness δ_T of a fluid flowing along a flat warm plate, as a function of the distance x from the leading edge of the plate. The plate is at a uniformly elevated temperature $T_h > T_\infty$, the temperature of the surroundings. The flow velocity of the fluid with respect to the plate, at sufficient distance from the plate is v_∞.

The thermal boundary layer thickness for a plate with a limited temperature elevation region starting at distance x_0 from the leading edge of the plate, can be found in literature [17].

Temperature distribution

The basic principle of a calorimetric flow sensor is that there is a temperature distribution around a heating element, which is disturbed by a flow. By placing temperature sensors at positions in the fluid where the temperature is sensitive to the flow velocity, the disturbance is measured and the flow velocity can be determined from that measurement. Knowledge of the temperature distribution in the fluid is essential for design of this type of thermal flowsensors. A simple procedure is to assume that the heater as well as heat sinks (typically cold walls) have a uniform temperature. This is often reasonable, for example if the heater and the channel walls are metal or silicon. The heater and heat sink temperatures can be taken as boundary conditions in the calculation of the temperature profile. Once the temperature profile is known, the heat injection from the heater into the fluid can be calculated from the temperature gradients in the fluid next to the heater. The amount of

heat injection should equal the heat generated in the heater. From this balance the heater temperature and the amplitude of the temperature distribution in the fluid can be calculated. The amount of heat injection (power P) from a heated wire into a flow for fixed temperature elevation of the heater, in the vicinity of a heat sink is given by King's Law [1]:

$$P = \alpha\sqrt{Re} + \beta \tag{10}$$

For small flows, the heat loss is mainly determined by the heat conduction to the heat sinks. The heat convection increases with increasing flow, and above a certain critical velocity the convection will be the dominant mechanism. This is the working range of anemometer flow sensors. We will now analyze a configuration with a flat thin heater plate between walls (fig. 4), in order to explain: 1. The heat transfer from the heater to the heat sinks, which is needed to determine the relation between the heater temperature and the heating power. 2. For small flow velocities v, the temperature difference measured at fixed locations up- and downstream of the heater is proportional to v. Assume that both the heater and heat sinks have a uniform temperature, T_h and T_0 respectively. The configuration is thought to be infinite in the direction perpendicular to the plane of the drawing. For constant density of the fluid and neglecting viscous dissipation, the heat transfer is governed by the following differential equation [11]:

$$k\nabla^2 T - \rho c_p \cdot \boldsymbol{v} \cdot \nabla T = 0 \tag{11}$$

For a fluid with flow field $v(x,z)$ in the x-direction only, this reduces to:

$$k\nabla^2 T - \rho c_p \cdot v \cdot \frac{\partial T}{\partial x} = 0 \tag{12}$$

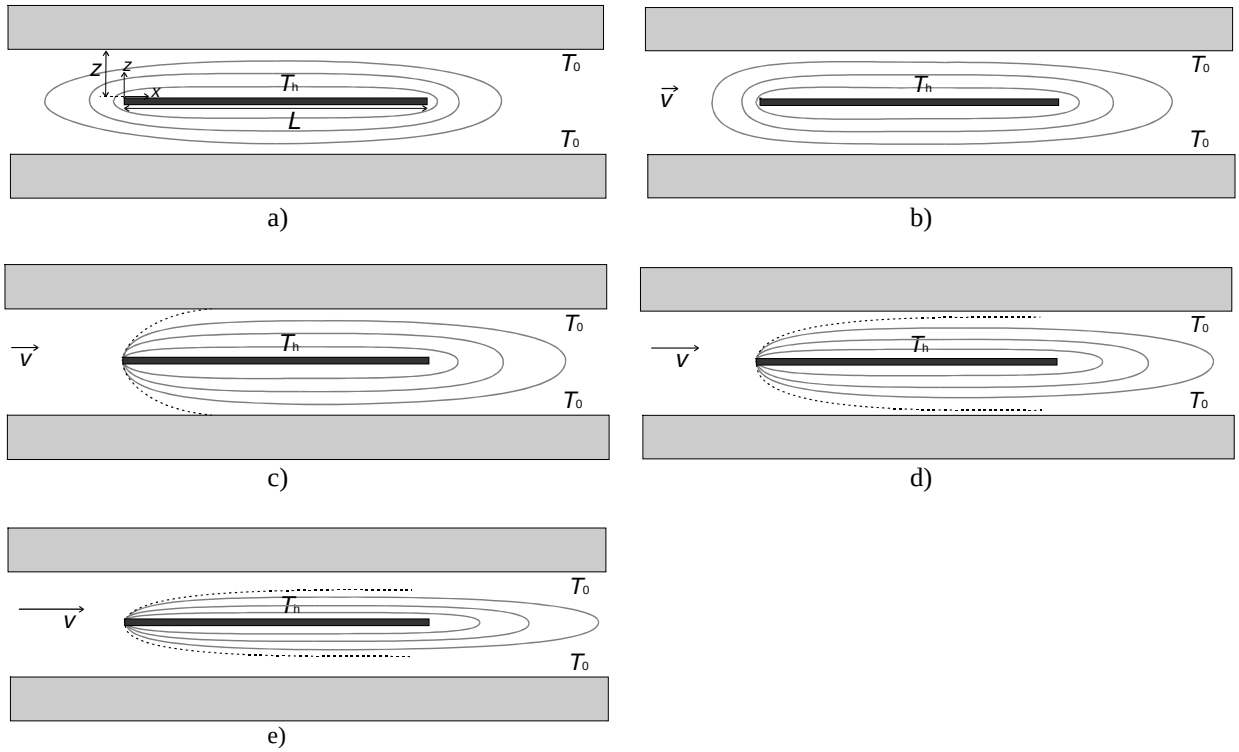

Figure 4: Heater plate in a rectangular channel. The distance to the wall is z, the length of the plate is L. a) Zero flow, the temperature distribution is symmetrical. b) Small v, up-stream the isothermal lines are compressed, down-stream they are stretched, the deformation is odd in x. Between the plate and the walls the temperature profile remains unchanged. c) The boundary layer extends between the heater and the walls. For constant temperature the heat injection increases. d,e) For increasing v the boundary layer extends over the whole heater. The boundary layer thickness decrease with $1/\sqrt{Re}$, therefore the heat transfer with $\sqrt{Re}$, following King's Law.

For small v ($Re < 1$) it can be shown that the flow field has a fixed shape function multiplied by the velocity amplitude v_m, which is the mean flow velocity over the cross section of the channel. This is the *creeping flow* regime [11], where the inertial effects are negligible. For steady state, Navier-Stokes equations again reduce to eq. (1). For creeping flow there are still entrance effects, however the shape of the velocity distribution remains constant. In this regime the temperature distribution in the fluid can be composed of the profile $\Gamma_0(x, z)$ for $v = 0$, with a disturbance function Γ_v (v_m, x, z) superimposed [10]. The amplitude of this disturbance function is proportional to v_m. For configurations with mirror symmetry in x-direction with respect to the heater, this implies that Γ_v is an odd function in x (with respect to the middle of the heater). The proportionality with v_m can be shown as follows: Let $T = \Gamma_0 + \Gamma_1$ be the solution of eq. (12) for a certain $v = v_1$. This implies that ($\forall x, z$):

$$k\nabla^2\Gamma_1 - \rho c_p \cdot v_1 \cdot \frac{\partial(\Gamma_0 + \Gamma_1)}{\partial x} = 0 \qquad (13)$$

If for $v_2 = \varepsilon \cdot v_1$ ($\varepsilon>0$) $T(v_{m2}, x, z) = \Gamma_0 + \varepsilon \cdot \Gamma_1$ is a solution then $T(v_{m2}, x, z)$ should be a solution to eq. (12):

$$\varepsilon \cdot k\nabla^2\Gamma_1 - \rho c_p \cdot \varepsilon \cdot v_1 \cdot \frac{\partial(\Gamma_0 + \varepsilon \cdot \Gamma_1)}{\partial x} = 0 \qquad (\forall x, z) \qquad (14)$$

With eq. (13) it becomes immediately clear that this is true for sufficient small $v_2 = \varepsilon \cdot v_1$ such that the third term in eq. (14), which is quadratic in ε, can be neglected. Because of the symmetry, for small v the increase of the temperature gradient next to the heater up-stream, will be equal to the decrease of the temperature gradient next to the heater down-stream (fig. 4b). For constant temperature the total heat injected from the heater is therefore constant ($\partial P / \partial v = 0$). Note that this is in conflict with King's Law, which predict an infinite $\partial P / \partial v$ at $v = 0$. There is experimental data which seems to confirm the deviation from King's Law for low Re [9, 18]. Although the heater temperature remains constant for small v, the temperature distribution in $+x$ and $-x$ direction can already be changed significantly. The temperature elevation extends in the channel in the x-direction typically over a distance of a few times z (fig. 4a,b). from the heater. Temperature sensors should be placed on up-and downstream locations with a large $\partial T / \partial v_m$. These are located typically around a distance z away from the heater. For increasing v the densification of the isothermal lines will enter the gap between the heater plate and the walls. If the boundary layer extends across a significant length $x_c = a \cdot L$ into the gap, then the heat conduction will significantly increase (Fig. 4c and Fig. 5). In the region where the boundary layer is thinner then z, the temperature gradient in both $+z$ and $-z$ direction next to the plate increases.

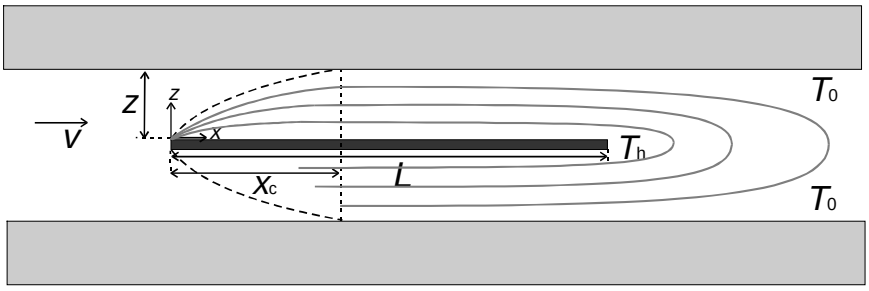

Figure 5: For sufficiently high flow speed (in $+x$ direction) the densification of the isothermal lines enters the gap between the heater plate and the walls. The boundary layer touches the wal at a distance x_c from the leading edge of the plate. The heater plate has a length L and the gap between the plate and the cold walls is z.

Using eq. (7) for the thermal boundary layer thickness it follows easily that the convective cooling becomes significant for:

$$\frac{d}{Re_z^{1/2} \cdot Pr^{1/3}} \cdot \sqrt{\frac{a}{b}} = 1 \qquad (b < 1, Pr \geq 1) \qquad (15)$$

Where $b = z / L$, and d a dimensionless constant (≈5). We should note that the boundary layer theory presented before is based on a uniform flow velocity outside the vicinity of the plate, therefore in this configuration (inside a channel) it can

only be used for an estimation. Also we assume that *Re* is low enough to have laminar flow. In the anemometer regime (a > 1), the boundary layer is the gap size across which $\Delta T_h = T_h - T_0$ drops (fig. 4d,e). According to eq. (7) the thickness of the whole boundary layer decreases with $1/\sqrt{Re}$, and therefore the heat transfer increases with $\sqrt{Re}$ (King's Law). Qualitatively it is now easy to draw $\Delta T = T_d - T_u$ vs. v for the heated plate with an up-stream temperature sensor (at T_u) and a down-stream temperature sensor (at T_d), located appr. at a distance z from the heater plate (fig. 6). The linear part for small v corresponds with fig. 4a,b, the part which follows the $1/\sqrt{Re}$ behavior corresponds with fig. 4d,e.

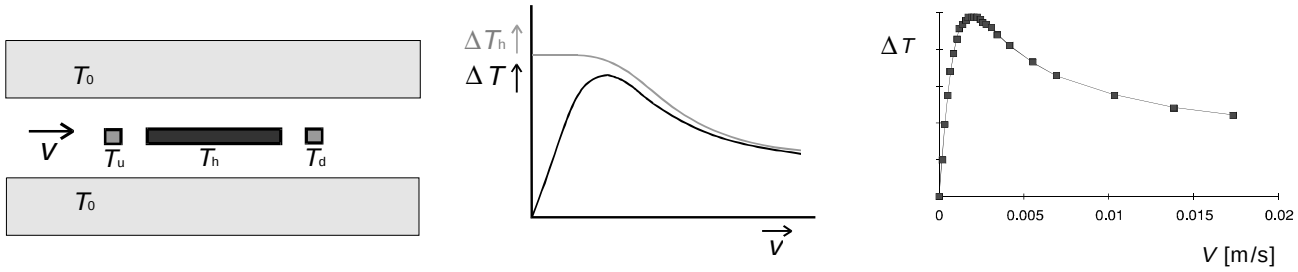

a) b) c)

Figure 6: a) Heated plate from fig. 4 and 5 in combination with an up-stream and down-stream temperature sensor (at T_u and T_d respectively). b) $\Delta T = T_d - T_u$ vs. v and $\Delta T_h = T_h - T_0$ vs. v for this configuration driven at constant heating power. c) Measured ΔT vs. v for water, constant heating power [8].

To calculate the temperature distribution in a flow sensor, it is sometimes possible to use a one-dimensional linear differential equation for the heat transport. In combination with an appropriate form of eq. (10) it is then easy to derive explicit expressions for the temperature distribution as a function of the flow velocity [8,19].

Estimation of sensor sensitivity

The sensor sensitivity in the end depends on the signal to noise ratio at the sensor output. This of course depends on thermal and flow configuration, fluid properties, heating power, as well as the temperature sensors and read-out electronics used. Here we only estimate the sensor sensitivity $S_{\Delta T} = \partial (\Delta T) / \partial v_m$, where ΔT is the temperature difference between the down-stream and the up-stream temperature sensor. For a given configuration $S_{\Delta T}$ is a function of the fluid properties, and is proportional to the relative heater temperature $\Delta T_h = T_h - T_0$. If we assume that $\Delta T_{max} = \Delta T_h$ (up-stream -1/2 ΔT_h and down-stream +1/2 ΔT_h) and that this maximum is reached at v_{max} as determined by eq. (15) for the onset of convective cooling, we find with $b = 0.2$ and $a = 0.2$:

$$S_{\Delta T} = \frac{\Delta T_{max}}{v_{max}} \approx \frac{\Delta T_h \cdot \rho \cdot z \cdot Pr^{2/3}}{d^2 \cdot \mu} \qquad (16)$$

From eq. (16) it follows that for the same ΔT_h the sensitivity for liquids is usually much higher than for gasses (for water and air at 293 K the ratio is 53). However, the larger heat conductivity of liquids generally leads to lower heater temperatures ΔT_h, so practically a large part of the difference in sensitivity is lost.

Typical calorimeteric flow sensor configurations

In principle calorimetric flow sensors can be made using one heater and one temperature sensor located either up-steam or down-stream of the heater (fig. 7a). The disadvantage of this configuration is that the absolute temperature is measured, which makes this configuration sensitive to variations of the temperature of the medium and/or the heat sinks. To reduce this undesirable sensitivity it is advantageous to do a differential measurement, using a temperature sensor to measure the temperature of the fluid far away from the heater (fig. 7b) [20]. This reference sensor can also be placed near the heater, so that its signal contributes to the output signal (fig. 8). The number of transducer elements in this configuration is three. Note that in fig. 9c the heater and sensor bridges are separated. This is done to reduce the parasitic conductance from the heater to the sensors through the bridge. Due to this conductance, the configuration of fig. 9b had a reduced sensitivity, especially with air as the flow medium [8]. The number of transducer elements can be reduced if the heater and temperature sensor are spatially integrated. A configuration with two sensor/heater elements is then enough to do a differential temperature measurement (fig.9). Due to the linearity of the heat transport equation, it is allowed to superimpose the temperature profiles of the two heaters driven at known heating powers. In this configuration the heater temperatures become dependent on the

flow velocity, also in the low velocity regime, because of the mutual sensitivity of heater/sensor 1 on the temperature profile generated by heater/sensor 2, and vice-versa. With resistive elements, heater and sensor can be integrated in one and the same wire. For both the amplitude of the temperature elevation (heater function) as well as the temperature sensor sensitivity, it is then advantageous to choose a large current [21]. In a three beam configuration, where heater and sensor function are spatially separated, the sensing current should be kept small, in order not to disturb the temperature distribution generated by the heater. The larger possible measurement current in the two beam configuration gives a higher possible signal to noise ratio. In fig. 9b,c the heaters and sensors close together, but still separated. In fig.14, section 5, a two beam sensor with heating/sensing function integrated in one wire on each beam is shown.

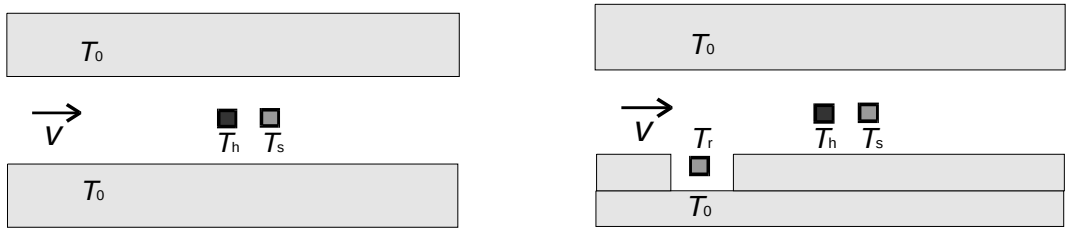

a) b)

figure 7: a) Calorimetric flow sensor with one heater and one temperature sensor. b) To reduce the sensitivity to variations in the incoming fluid temperature, it is advantageous to do a differential measurement, using a temperature sensor to measure the temperature of the fluid far away from the heater [20].

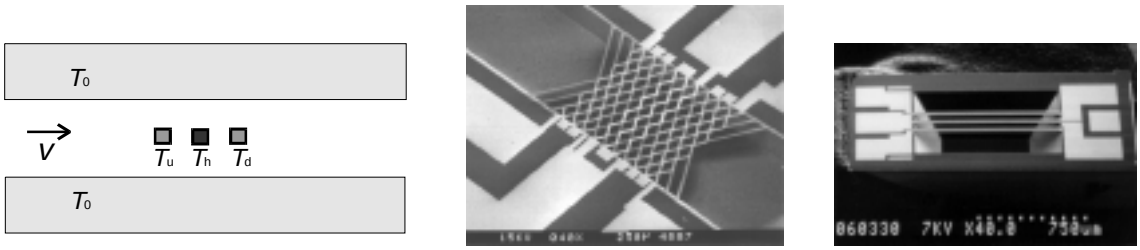

a) b) c)

Figure 8: a) the reference temperature sensor can be placed near the heater to contribute top the output signal b) SEM-photograph of the micro flow sensor structure with three meander shaped thin film resistors[8] c) Three element flow sensor, with separate bridges to reduce heat conduction between the elements [19].

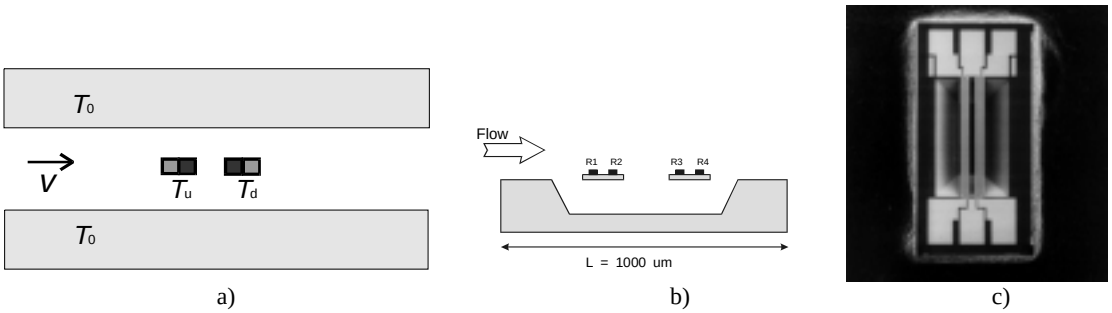

a) b) c)

Figure 9. a) Up-and down-stream sensors and heaters are spatially integrated b) Cross section of a two beam flow sensor, with heater/sensor pairs combined on two bridges. c) SEM-photograph of this two beam sensor. The resistors are supported by 80 μm wide silicon nitride bridges at 40 μm distance from each other [19].

3. Thermal-Electric Transducers

Temperature sensors are discussed only briefly here. We refer to Meijer [22] for an extensive general overview, Jiang [23] for extensive treatise on thin film thermistors, and Castano [24] for high figure of merit thin-film thermocouples. Three widely used transducer principles are compared in table 2: The RTD (Resistance Temperature Detector), Thermistor and Thermocouple.

	Thermocouple	RTD	Thermistor
Temperature range	-400..1500 ^{0}C	-200 .. 850 ^{0}C	-50 200 ^{0}C [1]
linearity	0	++	--
stability	--	++	0
Sensitivity	-- [2]	0 [2]	++ [2]
Consist from	Metals and/or semiconductors	Metals	Semiconductors
Temperature reference needed ?	Yes	No	No
Transducer type	Generator	Modulator	Modulator
Physical background	Seebeck effect	Electron scattering by lattice vibration	Free carrier generation
Temp measurement	Differential	Absolute	Absolute

Table 2: Data on temperature sensing principles compared.
[1] Estimated from [25]
[2] See text for discussion

Important issues for selection are the difficulty of fabrication, range, sensitivity and signal to noise ratio's of the respective principles. Based on own experience we restrict the discussion to a comparison of RTD and thermocouples. The differences in physics involved make a comparison on sensitivity difficult. However when assumptions are made about maximum voltages and circuits used, one can compare the sensitivity. For the RTD it can be shown that with a relative temperature coefficient of 1..5 10^{-3} [K^{-1}] and a maximum supply voltage of about 10 [V] the voltage variation caused by a certain temperature variation in a simple wheatstone geometry is about 10 to 50 [mV/K]. In comparison, a single all metal thermocouple will produce 10 to 100 [μV/K]. Off course a thermocouple of semiconductor material in combination with a metal has a much higher sensitivity of about 500 to 1000 [μV/K]. But even those thermocouples have to be arranged in a pile formation to obtain a sensitivity as high as the RTD. The noise-voltages and -currents for both thermocouple and RTD may expected to be mainly Johnson (or resistance noise), as described by the following equation:

$$U_n^2 = 4 \cdot k \cdot T \cdot R \cdot \Delta f \qquad (17)$$

With U_n the average noise voltage amplitude, k Boltzmann's constant, and Δf the bandwidth [Hz]. If we assume that thermopiles have a larger length when compared with RTD's (because they have to connect to a hot and a cold side), then the thermocouple metal should have either a larger thickness or width, in order to have an equivalent amount of noise. In conclusion, thermopiles will often take-up a significant larger space than RTD's. Based on the previous discussion, we may conclude that:

- Thermocouples are advantageous for a reduction of offset (only output voltage when a temperature *difference* is present)
- When its possible to stack many couples into a pile it's possible to obtain a high sensitivity but in general this means a relatively large transducer will be created.
- The RTD is advantageous to be used when small space is available, or absolute temperature measurement is required.

4. Measurement Methods and Systems

Within a thermal flow sensor configuration we need at least two transducers, a heater and a temperature sensor. The direct function of the heater is the generation of heat. This heat will result in a flow dependent temperature distribution with respect to space or time. Here we focus on time-independent (DC-flow modulated) temperature distributions. The function of the temperature sensor than is to monitor the temperature at a specific point in space. So the thermal flow sensor can be regarded is a stimulus-response measurement system which generates information about the flow (fig. 10).

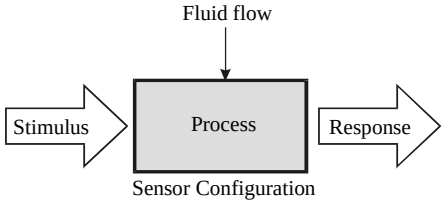

Figure 10: Thermal flow sensor as a stimulus-response system which generates information on the fluid flow. The stimulus consists of one or more power signals to the heaters and a resulting energy transport. The response of the configuration consists of one or more flow modulated temperature signals.

There is a wide variety of sensor systems with different ways of generating the stimuli and ways of measuring the response. The sensor systems can be categorized according to the way the different transducer signals are measured and controlled. A detailed analysis of various flow measurement systems and concepts is given by van Oudheusden and Lammerink [19, 20]. In this section we will discuss three basic sensor concepts.

In a **CPA** (Constant Power Anemometry) sensor system the power signal to the heater is kept at a constant value (see figure 11). With a constant power, the temperature sensor signal will decrease with increasing flow velocity v.

The fluid flow can be determined from the difference between the output signals from temperature sensor T_1 (signal U_1) and from ambient temperature sensor T_a (signal U_a), which then is calculated back (via m_{CP} and P_1) to obtain v^*. By using a small signal analysis Lammerink showed that a variation of the output signal dv^* becomes independent from an ambient temperature variation dT_a, when the temperature sensor sensitivities $m_1=\mathrm{d}U_1/\mathrm{d}T_1$ and $m_2=\mathrm{d}U_2/\mathrm{d}T_a$ are the same, while the temperatures T_1 and T_a are different. The temperatures T_1 and T_a can be measured with two absolute temperature sensors or with one differential temperature sensor (see section 3). In many CPA sensor systems a simpler approach is followed. Either the voltage or the current through the heater is kept constant and the variation in the applied power is corrected for.

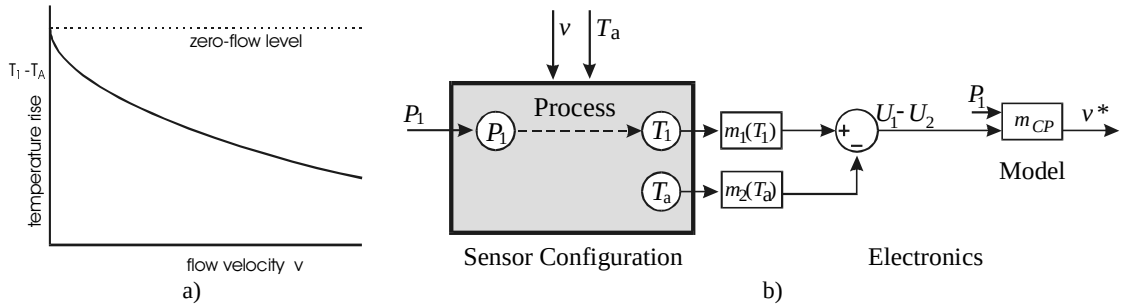

Figure 11: a) The physical model of the CPA sensor configuration according King's law. b) System structure of the CPA flow sensor system with the sensor configuration and the read-out electronics.

In a **CTA** (Constant Power Anemometry) sensor system the temperature (signal) of the temperature sensor T_1 is kept at a constant value above the ambient temperature T_a by means of an electronic controller (see figure 12). The heating power P_1 needed to keep the temperature sensor at a constant value above ambient will increase with increasing flow v.

With sufficient large gain of the control loop (β in figure 12b) the needed heating power P_1^* is a measure for the flow. The fluid flow can be determined from the P_1^* signal, which then is calculated back (via m_{CT} and U_{offset}) to obtain v^*. The sensor systems ouput signal v^* does not depend on the sensitivity $m_1(T_1)=\mathrm{d}U_1/\mathrm{d}T_1$ of the temperature sensor. Again it can be shown that a variation of the output signal dv^* becomes independent from an ambient temperature variation dT_a, when the temperature sensor sensitivities $m_1=\mathrm{d}U_1/\mathrm{d}T_1$ and $m_2=\mathrm{d}U_2/\mathrm{d}T_a$ are the same, while the temperatures T_1 and T_a are different. The temperatures T_1 and T_a can be measured with two absolute temperature sensors or with one differential temperature sensor (see section 3).

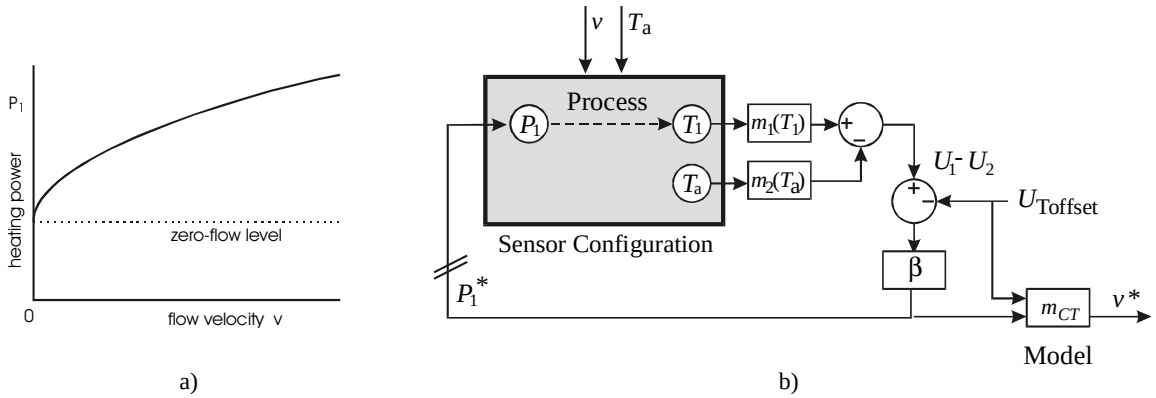

a) b)

Figure 12. a) Physical model of the CTA sensor configuration, according to King's Law. The power needed to keep the temperature sensor at a constant value above ambient will increase with increasing flow v. b) System structure of the CTA flow sensor system with the sensor configuration, the electronic control loop and the read-out electronics.

In a **TBA** (Temperature Balance Anemometry) sensor system temperature signals from temperature transducers are kept equal with help of a differential control loop (see figure 13). With the two temperatures T_1 and T_2 equal, and assuming a linear thermal behavior of the sensor configuration, the relative power difference $(P_1\text{-}P_2)/(P_1+P_2)$ of heater/sensor P_1/T_1 up-stream relative to heater/sensor P_2/T_2 down-stream will increase with increasing flow velocity v (figure 13a). Again with sufficient large gain β of the now differential-control loop the differential power signal ΔP^* is a measure for the flow and will be independent from the temperature sensor sensitivities $m_1=\mathrm{d}U_1/\mathrm{d}T_1$ and $m_2=\mathrm{d}U_2/\mathrm{d}T_2$. The fluid flow can be determined from the signal ΔP^* which is calculated back (via m_{TB} and $P_t=P_1+P_2$) to obtain v^*. Now an output signal variation $\mathrm{d}v^*$ becomes independent from an ambient temperature variation $\mathrm{d}T_a$, when the temperature sensor sensitivities m_1 and m_2 are the same, while the temperatures T_1 and T_2 kept equal due to the control loop. This implies that non-linear (though symmetrical) temperature sensors can be used. The temperatures T1 and T2 can be measured by either two absolute temperature sensors or a thermocouple (see section 3). An advantage of a thermocouple as a temperature sensor is that it has an intrinsic zero offset which means that $m_1(T)=m_2(T)$ for all temperatures T. First experiments on the TBA concept were done by Lammerink in which he verified the concept [19]. He also demonstrated a relative simple to implement oscillating differential-power controller.

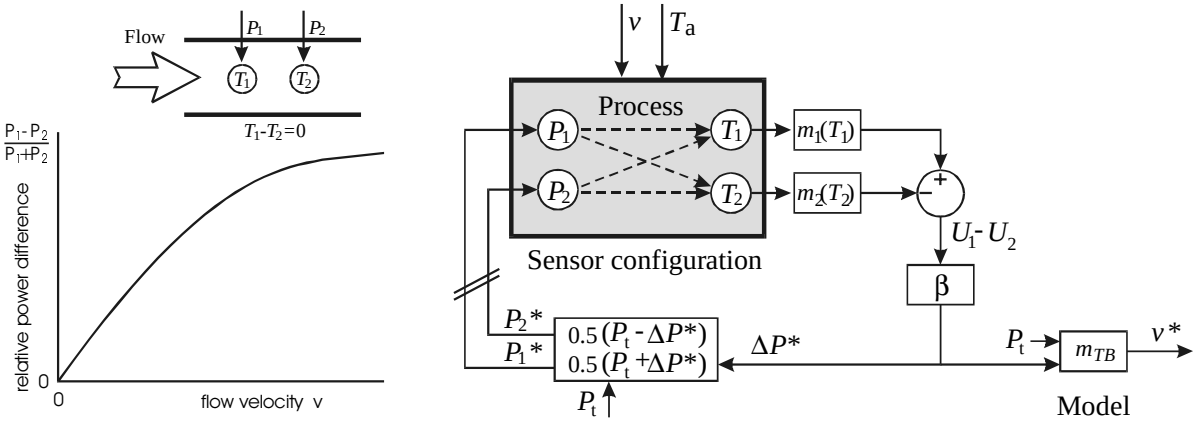

a) b)

Figure 13: a) The physical model for the relative power difference $P_1\text{-}P_2/P_t$ assuming a mutual thermal interaction and linear thermal behavior. b) System structure of a TBA sensor system with the sensor configuration, the differential control loop and the readout electronics. The total power $P_t=P_1+P_2$ distributed by the control loop is kept constant.

5. Acoustic Measurements

The Microflown is an acoustic sensor based on the calorimeter principle [26]. Nowadays sound-energy determination, array and three-dimensional impulse response are under investigation. Although the Microflown is invented relative a short time ago [27]), the device is already commercially available [28]. Since its invention it is mostly used for measurement purposes, 1D and 3D-sound intensity and acoustic impedance determination [29]. Instead of sound pressure, the Microflown is capable of measuring particle velocity, which is closely related to (sound) pressure gradient. So in an audio perspective the Microflown can be seen as a pressure gradient microphone (with a figure-of-eight directivity pattern) that has a good signal to noise ratio from 0Hz up to 1kHz. For frequencies higher than 1kHz the frequency response has a decay. The Microflown itself consists of two very closely spaced thin wires (spacing 350μm) of silicon nitride with an electrically conducting platinum pattern on top of them. SEM photographs of two types of Microflowns is depicted in fig. 14. The size of the two wires is 1000×10×0.5 μm (l×w×h). The metal pattern is used as temperature sensor *and* heater. The silicon nitride layer is used as a mechanical carrier for the platinum resistor patterns. The sensors are powered by an electrical current, causing the sensors to heat up. For small enough particle velocity amplitude (< 1 m/s or 146 dB PVL, re. 50 nm/s) the temperature difference of the two cantilevers is linear dependent on the particle velocity. The measured temperatures in a Microflown in operation are shown in fig. 15. The difference signal of both sensors represents the particle velocity, and the sum (the common temperature) the convective cooling down of the device.

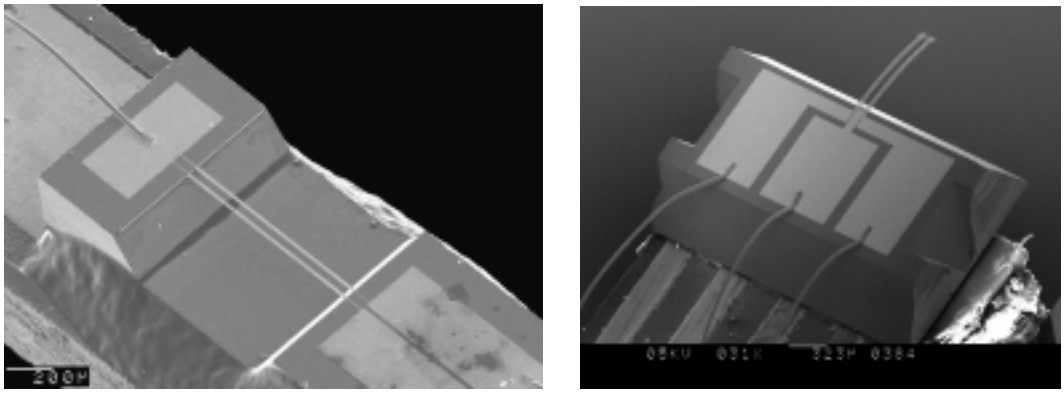

a) b)

Figure 14: a) SEM Photo of a part of a bridge type of Microflown. At the top of the sample a wire-bond is visible. The sample is glued on a printed circuit board, the glue can be seen at the side of the sample. b) SEM photo of a cantilever type of Microflown.

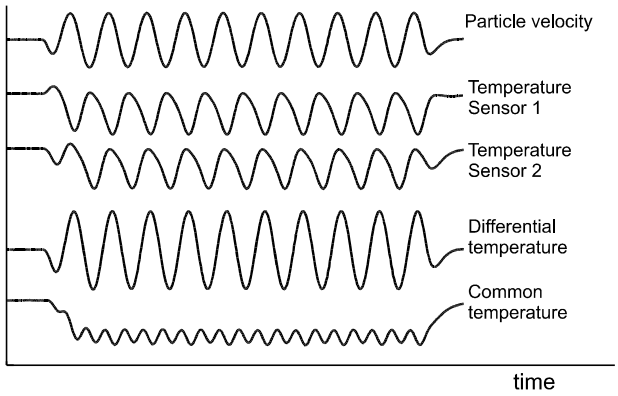

Figure 15: The (measured) temperatures of the Microflown as result of a particle velocity wave [30]. A particle velocity wave will cool down both sensors in a different manner. The difference signal of both sensors represents the particle velocity, and the sum (the common temperature) the convective cooling down of the device.

sensitivity

The sensitivity of a Microflown element itself is defined by the differential resistance variation of both sensors due to a particle velocity of 1m/s; that is 146dB PVL re. 50nm/s. At a power dissipation of 40mW to 60mW the sensitivity of a non-packaged Microflown is about 35‰; when packaged, the sensitivity rises about 15dB (5.5×) to 200‰. At 94dB (the acoustic reference level) the particle velocity is 2.5mm/s, the differential resistor variation at this velocity is 0.5‰. Calculations show that at low frequencies the Microflown should have a theoretical maximal S/N of (P=20mW per sensor, $T_{sensors}$=600K, the sensitivity at 94dB is ΔR/R=0.5‰) [21]:

$$\frac{S}{N} = 20Log_{10}\frac{1}{\sqrt{4k}}\cdot\frac{1}{\sqrt{Bw}}\cdot\sqrt{\frac{2P}{T_{sensors}}}\cdot\frac{\Delta R}{R}$$
$$= 20Log_{10}\frac{1}{\sqrt{4\times1.38\cdot10^{-23}}}\cdot\frac{1}{\sqrt{1[Hz]}}\cdot\sqrt{\frac{0.04[W]}{600[K]}}\cdot0.5\cdot10^{-3} = 115dB/\sqrt{Hz} \quad (18)$$

.

Measured frequency response

As an example, the frequency response of a so-called add-on Microflown [31] is depicted in fig. 16. It has been measured under anechoic conditions which means that sound pressure and particle velocity can be compared with each other in a proper way. The add-on Microflown is a studio microphone that is used to transduce the lower part of the audio bandwidth (16Hz-250Hz) since pressure gradient microphones are not able to cover this part.

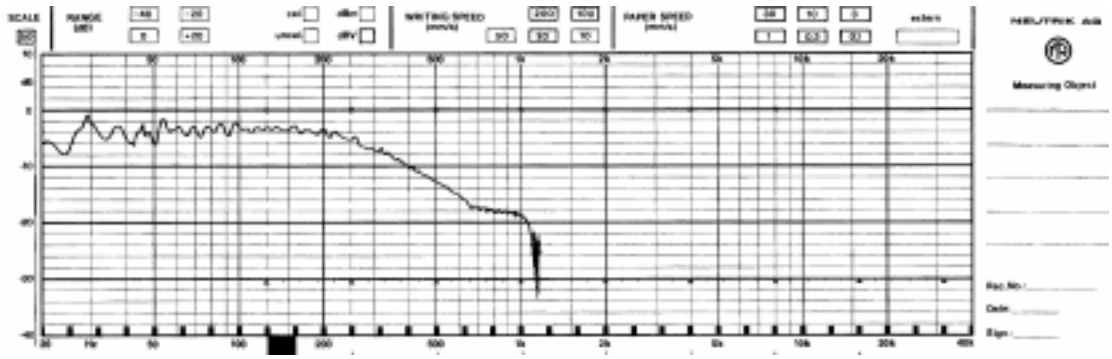

Figure 16: Frequency response of an add-on Microflown (with low pass-filter at 250Hz) [31].

Measured noise

To get an insight of the noise behaviour of the Microflown, no external and internal filtering has been utilised for the spectral density measurement. As can be seen in fig. 17, the spectral noise density of the add-on Microflown is about -102dBV at lower frequencies. The sensitivity was adjusted to 1V/94dB (94dB equals 2.25mm/s), the signal to noise ratio is measured 102dB/√Hz in stead of the 113dB/√Hz that was expected from theory (sensor+pre-amplifier). As can be seen the noise density is increasing at lower frequencies. It may be that some acoustic noise influenced the noise measurements. In conclusion, in a 1Hz bandwidth, 22.5nm/s is the equivalent noise level, which is a lower limit for the sensitivity.

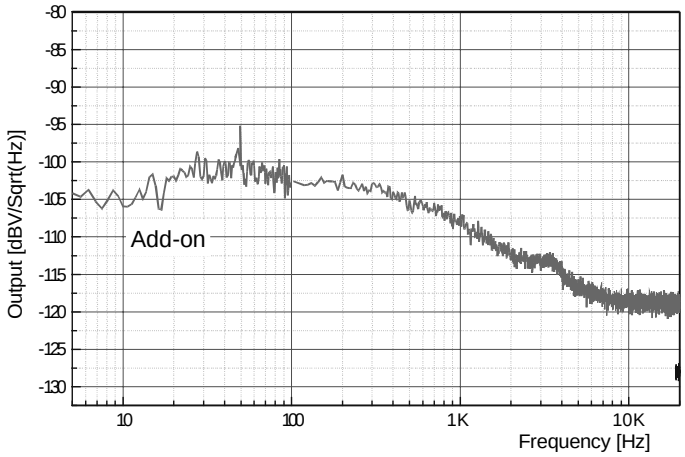

Figure 17: Noise density of the add-on Microflown [31] (the sensitivity of microphone was adjusted to 1dBV per Pascal).

6. Towards pL/s resolution

We are working on flow sensors for application in MICS (Micro Chemical Systems). Guiding dimensions for this application are (liquid handling): Reaction volumes in the order of $(0.1\ \text{mm})^3$, available driving pressures of 0.1 Bar and volume flows up to 1 nL/s. This latter flow rate corresponds with a flush-time of 1 s for the $(0.1\ \text{mm})^3$ volume. The flush-time is chosen in correspondence with typical reaction times of diffusion limited processes on sub-mm scale [32]. The 1 nL/s flow in combination with a maximum pressure drop of 0.1 Bar, yields an allowed flow resistance $R = 1 \cdot 10^{16}\ \text{Nsm}^{-5}$ of the flow sensor. For water this corresponds with a channel with length of 0.6 mm, width of 100 μm, and a height of 2 μm. For fabrication of liquid handling systems with these narrow channels we are working on a surface micromachining based technology (fig. 18): It is based on deposition and patterning of thin films of polysilicon and silicon nitride. Deep, low resistance connection channels are made by KOH etching of the silicon substrate wafer. This etching is preceded by KOH etching of a sacrificial polysilicon layer [33].

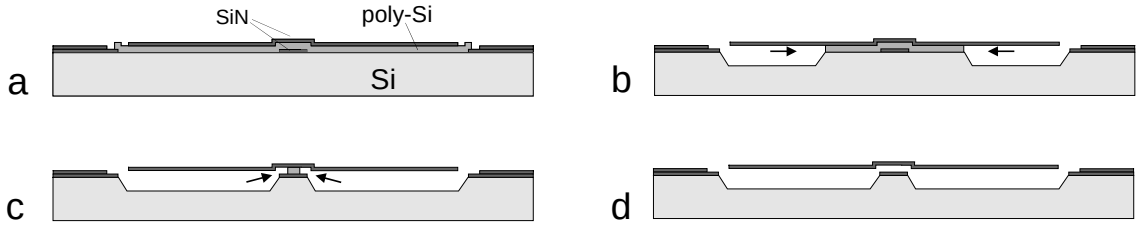

Figure 18: Etching of narrow channels and v-grooves using sacrificial layer etching of polysilicon. a) Polysilicon is sandwiched between two silicon nitride layers for making a narrow channel, and only covered on top with silicon nitride for making the v-grooves. b) The polysilicon etches, and exposed silicon of the substrate etches as well to form the v-grooves. c) The KOH reaches the polysilicon sandwiched between two silicon nitride layers. The narrow channel is etched. d) The narrow channel has been completed.

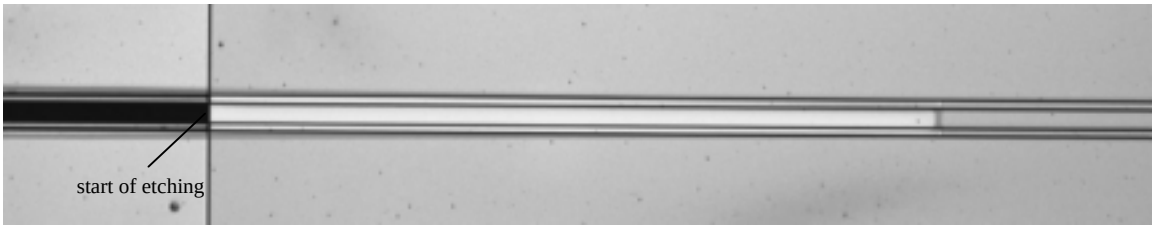

Figure 19: Top view of a channel with v-grooves, etched over a length of 1.1 mm. The lateral etch-rate was 1.6 μm/min., 25 wt% KOH at 74 °C. The polysilicon in this experiment was 2 μm thick.

Experiments show that it is possible to etch a 2 μm polysilicon layer sandwiched between two silicon nitride layers across distances up to 2 mm (fig. 19), without significant decrease of the etching speed with increasing length of the polysilicon track. The measured lateral etch-rate of the polysilicon is 1.6 μm/min. in 25 wt% KOH at 74°C, both for sandwiched polysilicon and v-grooves. Based on the example with a channel heigth of 2 μm and a channel width of 100 μm, a volume flow of 1pL/s corresponds with an average flow velocity of 5 μm/s in the flow sensor. Compared to the 23 nm/s equivalent noise level in air of the microflown this indicated that pL/s is feasible. Note that for the same temperature elevation the sensor is more sensitive for water as a medium. However, the hundreds of Kelvins temperature elevations are not feasible in water. Practically the sensitivity will be comparable for air and water.

7. Conclusions

For a proper design of thermal flow sensors it is important to look both at the internal flow and thermal properties, as well as the external properties of the flow sensor as a hydraulic system component. Beside thermal modeling, significant part of the paper has therefore been devoted to the hydraulics of micro flow sensors. Using the knowledge of the hydraulics it is possible to decrease the diameter of the flow channel of the sensor, in order to increase the flow velocity for a given volume flow. In the modeling section we showed why the calorimetric flow sensor has a linear response $\Delta T(v)$ for small v: The zero flow temperature distribution is disturbed in such a way that (for a symmetrical configuration) the up-stream decrease of the temperature equals the down-stream increase of the temperature. The overall heat transfer from the heater to the heat sinks therefore remains constant. This implies that for low *Re* a modification of King's Law has to be considered. The heater cools down by convection only when the non-linear disturbances come into play. Different measurement methods have been discussed: absolute, differential, constant power, constant temperature, and thermal balance measurements. The latter method has an attractive property for high sensitivity applications: It allows the use of non-linear temperature sensor elements. From our experience with thermal flow sensors used as microphone, we can estimate practically attainable sensitivities: The microflown measures air-flow velocities lower than 1 μm/s. In combination with the fabrication technology we are working on for the fabrication small volume micro-chemistry systems, this gives a promising perspective for the reach of pL/s sensitivity.

8. Acknowledgement

The authors would like to thank dr. ir. Frank Wisselink, currently with KPN Telecom, Marketing, The Hague, for helpful discussions about the fluidic and thermal modeling. Also we are grateful to ir. Joost van Honschoten for his advice on the thermal modeling.

9. Literature

1. King L.V.,"On the convection of heat from small cylinders in a stream of fluid: Determination of the convection constants of small platinum wires with application to hot wire anemometry", Phil. Trans. Roy. Soc. *A* (London), Vol. 214, 1914, pp. 563-570 (373-?).
2. van Putten A.F.P., Middelhoek S.,"Integrated silicon anemometer", Electr. Letters, 17th Oct. 1974, vol. 10, no. 21, pp. 425-426.
3. Petersen K., Brown J., Renken W.,"High precision, high performance mass-flow sensor with integrated laminar flow micro-channels", Proc. 1985 Int. Conf. on Solid-State Sensors and Actuators (Transducers '85), pp. 361-363.
4. Tai Y.C., Muller R.S., Howe R.T.,"Polysilicon-Bridges for Anemometer Applications", Proc. 1985 Int. Conf. on Solid-State Sensors and Actuators (Transducers '85), pp. 354-357.
5. Johnson R.G., Higashi R.E., Bohrer P.J., Gehman R.W.,"Design and packaging of a highly sensitive microtransducer for air flow and differential pressure sensing applications", Proc. 1985 Int. Conf. on Solid-State Sensors and Actuators (Transducers '85), pp. 361-363.
6. Bradshaw P.,"Thermal methods of flow measurement", J. Phys. E., ser. 2, vol. 1, 1968, pp. 504-509.
7. van der Wiel A.J., Hoogerwerf A.C., de Rooij N.F.,"A calorimetric mass-flow sensor for hostile environments", 7th Int. Conf. on Solid-State Sensors and Actuators (Transducerss '93), Pacifico, Japan, June 7-10 1993, pp. 800-803.
8. T.S.J. Lammerink, N.R.Tas, M. Elwenspoek, J.H.J. Fluitman,"Micro-liquid Flowsensor", Sensors and Actuators, A 37-38, 1993, pp. 45-50.
9. Wu S., Lin Q., Yuen Y., Tai Y.C.,"MEMS Flow Sensor For Nano-Fluidic Applications", IEEE MEMS Conf. 2000, Miyazaki, Japan, Jan 23-27 2000, pp 745-750.
10. Elwenspoek M., Wiegerink R.J.,"Principles of Mechanical Microsensors", Springer Verlag, to be published in 2000.
11. Bird R.B., Stewart W.E., Lightfoot E.N.,"Transport phenomena",John Wiley & Sons, New York, 1960.
12. Kays W.M., Crawford M.E.,"Convective heat and mass transfer", McGraw-Hill, NewYork, 1993.

13. Tas N.R.**,** "Design and Realization of a micromachined hydraulic astable multivibrator", M.Sc. Thesis Uiversity of Twente, Dept. Electrical Engineering, November 1994.
14. Shah R.K., London A.K.,"Laminar flow forced convection in ducts", Academic Press, New York, 1978.
15. Urbanek W., Zemel J.N., Bau H.H.,"An investigation of the temperature dependence of Poiseuille numbers in microchannel flow", J. Micromech. Microeng. 3 (1993) pp.206-208.
16. Lammerink T.S.J., Tas N.R., Berenschot J.W., Elwenspoek M., Fluitman J.H.J.,"Micromachined Hydraulic astable multivibrator", Porc. IEEE MEMS Workshop1995, Amsterdam , the Netherlands, Jan. 29 - Febr. 2 1995, pp. 13-18.
17. Menendedez A.N.**,**"The use of flush-monted hot-film gauges to measure skin friction in unsteady boundary layers", J. Fluid Mech., Vol. 161, 1985, pp. 139-159.
18. de Bree H-E., Jansen H.V., Lammerink T.S.J., Krijnen G.J.M., Elwenspoek M.,"Bidirectional fast flow sensor with a large dynamic range", Proc. 9th Micromechanics Europe Workshop (MME '98)", Ulvik in Hardanger, Norway, June 3-5 1998, pp. 194-197.
19. Lammerink T.S.J., Tas N.R., Krijnen G.J.M., Elwenspoek M.," A new class of thermal flow sensors using ΔT=0 as a control signal", IEEE MEMS Conf. 2000, Miyazaki, Japan, Jan 23-27 2000, pp.525-530.
20. van Oudheusden B.W., " Silicon thermal flow sensors"**,** Sensors and Actuators, A 30, 1992, pp. 5-26.
21. H.E. de Bree, Leussink P., Korthorst T., Elwenspoek M.,"The two sensor micro-flown", Proc. Eurosensors X Conf., Leuven, Belgium, Sept. 8-11 1996, pp. 1301-1304.
22. Meier G.C.M., Herwaarden A.W.,"Thermal Sensors", Institute of Phys. Publishing, Bristol, 1994, ISBN 0-7503-0220-8.
23. Jian L., Wong M., Zohar Y.,"Micromachined polycrystalline thin film temperature sensors", Meas. Sci. Technol., vol. 10, 1999, pp. 653-664.
24. Castaño E., Revuelto E., Martin M.C., Garcia-Alonso A., Garcia F.J., "Metallic thin-film thermocouple forthermoelectric microgenerators," *Sensors and Actuators A* 60 pp.65-67, (1997).
25. Rowe D.M.**,** CRC Handbook of ThermoElectrics, CRC press., Boca Raton 1995.
26. de Bree H-E., Leussink P., Korthorst T., Jansen H., Lammerik T.S.J., Elwenspoek M., The Microflown: a novel device measuring acoustical flows, Sensors and Actuators A 54 (1996) 552-557.
27. de Bree H-E., Lammerink, Elwenspoek, Fluitman, Patent PCT/NL95/00220, Use of a fluid flow measuring device as a microphone and system comprising such a microphone 1995.
28. Www.microflown.com
29. Druyvesteyn W.F., de Bree H-E., A new sound intensity probe; comparison to the Bruel & Kjaer p-p probe, 104th AES Convention Amsterdam; pre-print 4651, 1998
30. deBree H-E.,"The Microflown", Ph.D. Thesis Uiversity of Twente, 1997, ISBN9036509626.
31. de Bree H-E.,"Add-on Microflown for a high-end pressure gradient microphone", AES Conf. 2000.
32. Miyake R.**,** Lammerink T.S.J., Elwenspoek M., Fluitman J.H.J.,"Micro Mixer with fast diffusionn", Proc. IEEE MEMS Workshop 93, Fort Lauderdal, USA, Febr. 7-10 1993.
33. Sugiyama S., Suzuki T., Kawahata K., Shimaoka K., Takigawa M., and Igarashi I.,"Micro-diphragm pressure sensor", Proc. Int. Electr. Dev. meeting 1986, Los Angeles, CA USA, Dec. 7-10, 1986, pp. 184-187.